

# DETERMINATION OF INVERSE DEPTHS USING DIRECT BOUSSINESQ MODELING

By A. B. Kennedy,<sup>1</sup> R. A. Dalrymple,<sup>2</sup> Fellow, ASCE, J. T. Kirby,<sup>3</sup> Member, ASCE, and Q. Chen,<sup>4</sup> Associate Member, ASCE

**ABSTRACT:** This paper presents a technique to reconstruct bathymetry using two snapshots of water surface elevations and velocities as data. A Boussinesq model initialized with the data from the first snapshot is used as the engine to compute wave evolution over test bathymetries, which are iterated until a best fit is reached with the second snapshot. Phase speed difference in computed and measured data is used as the basis for updating bathymetry at each iteration. A novel technique is used to minimize the effect of mismatches between velocity and surface elevation, which could otherwise result in significant errors in phase speed estimates. The inversion algorithm is found to reconstruct bathymetries well for a variety of test cases. A particular strength of the methodology is the ability to account consistently for strong, unsteady currents while constructing the inverse bathymetry.

## INTRODUCTION

As waves approach a shoreline from deep water, they undergo strong changes. Wave lengths and phase speeds decrease and heights increase. Refraction and diffraction, nonlinearities, and breaking further affect wave properties. Most of these changes are caused either directly or indirectly by the bottom bathymetry acting on waves as they make their way toward the coast. A large amount of research has gone into the problem of predicting exactly what these changes will be, using many different techniques. Recently, Boussinesq-based numerical models have demonstrated the capability to predict a wide variety of nearshore processes with good accuracy (Madsen et al. 1997a,b; Kennedy et al. 2000; Chen et al. 1999, 2000). Given initial wave conditions, reasonable estimates of wave transformation and wave-induced currents may be found for complex topographies. Furthermore, because these are time stepping models, instantaneous snapshots of water surface elevations and velocities may be produced at any desired time.

However, little effort has been expended on the other side of the coin: Given spatial data on water surface elevations and/or velocities, find the bathymetry that would cause these properties. Based on the promise of modern airborne and satellite radar and altimeter platforms to provide dense spatial phase resolving estimates of surface elevations and/or velocities, interest in this topic has begun to increase.

Several depth inversion techniques have been developed, all based on the premise of spatially dense, remotely sensed measurements of surface elevations at two or more time intervals, which are then used to calculate, either explicitly or implicitly, phase speed. Wu and Juang (1996) used P-band satellite images over reasonably large-scale coastal regions to calculate the dispersion surface of the water using standard Fourier techniques. The linear dispersion relationship was then used to estimate depths. However, resolution was poor. Dugan et al. (1996) used an airborne infrared system to take a sequence of

images of the water surface. The 3D frequency-wavenumber spectra was then calculated, and depth was inferred using linear dispersion. Dalrymple et al. (1998) used synthetic data with several linear techniques, including spectrum reconstruction from cross-correlation functions, to estimate depths over 1D and 2D topographies. Good results were found but, as must be the case with all linear methods, accuracy deteriorated as wave heights increased. A method taking nonlinearity into account is that of Grilli (1998). Here, numerous runs from a 1D boundary element model were used to accumulate data on nonlinear dispersion. These data then were used to provide a methodology for estimating depths based on wave height, wavelength, and phase speed. However, the inversion as presented was only applicable to 1D, nonbreaking regular waves. Stockdon (1997) used land-based video images to calculate wavelengths and phase speeds in the nearshore and the linear dispersion relationship to infer the depth. Some success was found, but depths were significantly overpredicted.

All of these techniques used only measured surface elevation or phase data to perform inversions. Although this can provide good results for some cases, it has a major drawback; it cannot take into account the effect of currents on wave speeds. An opposing current, which will slow a wave's speed, would be interpreted instead as an underwater ridge, and a following current would become a trough in the inversion. However, methods that also use surface velocity data would correctly interpret these features. Furthermore, a method that includes breaking effects would be able to perform inversions consistently through the surf zone, instead of treating it as either a linear or nonlinear nonbreaking process.

This paper looks at what is essentially a best-case scenario: Can accurate depth inversions be performed when spatially dense surface elevation and velocity information is available? Based on the accuracy or inaccuracy of any such technique, it may then be possible in future work to make accurate approximations for the less optimal cases of surface elevation only, surface velocity only, or phase information only.

The technique developed here to reconstruct bathymetry uses two snapshots of water surface elevations and velocities and produces generally very good results. The second section looks at some general inversion principles and considers the suitability of Boussinesq models for inversion. The third section describes the depth inversion algorithm and particularly the depth updating procedure. A method to minimize the effects of errors in the data is also presented in this section. The fourth section shows the results of inversions using synthetic data for a variety of topographies and wave and current conditions. The final section discusses the results in more general terms and presents some conclusions.

<sup>1</sup>Postdoctoral Fellow, Ctr. for Appl. Coast. Res., Univ. of Delaware, Newark, DE 19716.

<sup>2</sup>Prof. and Dir., Ctr. for Appl. Coast. Res., Univ. of Delaware, Newark, DE.

<sup>3</sup>Prof., Ctr. for Appl. Coast. Res., Univ. of Delaware, Newark, DE.

<sup>4</sup>Postdoctoral Fellow, Ctr. for Appl. Coast. Res., Univ. of Delaware, Newark, DE.

Note. Discussion open until January 1, 2001. To extend the closing date one month, a written request must be filed with the ASCE Manager of Journals. The manuscript for this paper was submitted for review and possible publication on April 20, 1999. This paper is part of the *Journal of Waterway, Port, Coastal, and Ocean Engineering*, Vol. 126, No. 4, July/August, 2000. ©ASCE, ISSN 0733-950X/00/0004-0206-0214/\$8.00 + \$.50 per page. Paper No. 20743.

## SUITABILITY OF BOUSSINESQ MODELS FOR DEPTH INVERSION

There are both theoretical and practical limits to finding bathymetry from surface data. The first, and most obvious, is that, when the depth becomes too large, wave properties cease to depend on the bathymetry. The best example of this is the linear dispersion relationship

$$\frac{\omega^2}{gk} = \tanh(kh) \quad (1)$$

where the dimensionless depth  $kh$  is a function only of the dimensionless frequency,  $\omega^2/gk$ , which can be calculated from the measured frequency  $\omega$  and wavenumber  $k$ . Therefore, using the dimensionless frequency, which may be found from measured wavenumbers and frequencies, the inverse depth of water underneath the wave may be inferred. Fig. 1 shows the inferred dimensionless depth calculated from linear theory. For frequencies greater than about 0.95, or dimensionless depths greater than  $kh = 1.5$ , a small change in frequency causes a large change in depth, greatly magnifying any measurement error. Theoretically, given perfect data, inverse depths could still be obtained for even greater depths, but this may represent a practical limit given the inherent error involved in any such measurements.

Further limits are introduced by the Boussinesq approximation. For the model of Wei et al. (1995), the linear dispersion relationship is given by

$$\frac{\omega^2}{gk} = kh \frac{1 - kh^2(\alpha + 1/3)}{1 - kh^2\alpha} \quad (2)$$

where  $\alpha$  is a free parameter, which in all cases here is taken to be  $\alpha = -0.390$ , as recommended by Nwogu (1993). This dispersion relationship is only an approximation to (1), so inferred depths will also be in error. Fig. 2 shows the inferred depths using (2) compared to the exact depths calculated using (1). The Boussinesq model performs quite well up to dimensionless depths of about  $kh = 1.5$ , where it begins to deviate somewhat from the exact solution. However, this is already at the practical limit for inversion, so it does not represent a real problem.

The specific model used here is based on the fully nonlinear extended Boussinesq equations of Wei et al. (1995), with additions to include wave breaking and a shoreline condition as detailed in Kennedy et al. (2000) and Chen et al. (2000). This model predicts with good accuracy wave transformation

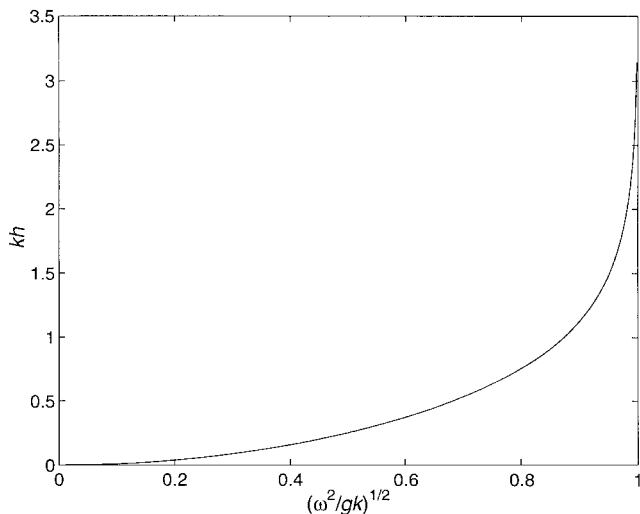


FIG. 1. Linear Dispersion Relationship, Showing Measured Frequency and Inferred Depth

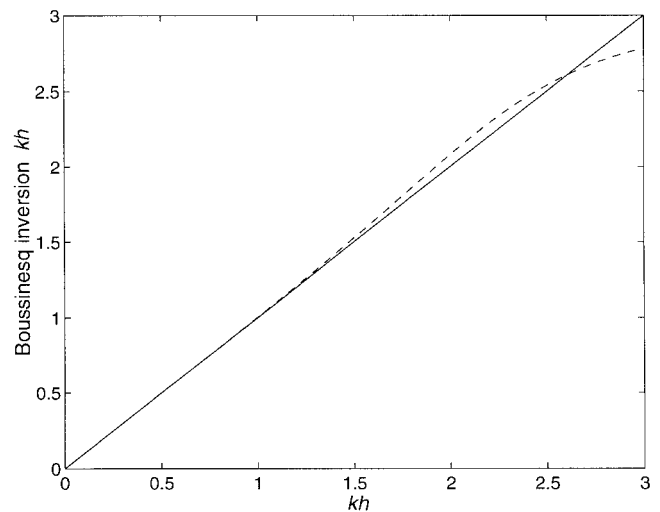


FIG. 2. Inferred Depths Using Boussinesq Dispersion (---), Compared to Exact Solution (—)

through the surf zone including breaking, runup, and wave-induced currents. Also, unlike many weakly nonlinear Boussinesq-type equations, it also predicts consistently wave-current effects, as shown in Kirby (1997). Therefore, it should be able to reproduce well the wave evolution as measured at subsequent snapshots, given correct initial conditions and the correct bathymetry.

## INVERSION TECHNIQUE

The framework for inversion is straightforward:

1. Take dense spatial measurements of free surface elevations and velocities over the area of interest at two times separated by  $<1$  dominant wave period.
2. Guess the initial bathymetry (flat bed chosen for all cases here).
3. Run the Boussinesq model using measured initial surface elevations and velocities and assumed bathymetry as the initial conditions.
4. Compute surface elevations and velocities at the second measurement time.
5. Compare measured and computed surface elevations and velocities at the final measurement time, and use this to update the assumed bathymetry.
6. If the bathymetry has not converged, go to Step 3; otherwise end the sequence.

The key to this framework is the procedure in Step 5 for updating the depth given the difference between the measured and computed quantities at the second measurement time. Based on a knowledge of wave behavior, a relatively simple method has been developed to update bathymetry that uses local phase speed as the decision criterion. This updating procedure is not specifically tied to the Boussinesq model used here. In fact, any desired wave driver could be used, with the final results dependent on the accuracy of the model and quality of the data.

## DEPTH UPDATING ALGORITHM

Because the assumed bathymetry, and the Boussinesq model, are not exact, there will be differences between computed and measured quantities at the second measurement time. The inversion task is to minimize these differences in some way by altering the assumed bathymetry. One possibility would be to minimize the square of the difference between

measured and computed values, summed over the entire domain. The inverse bathymetry would be that which minimizes this function. The minimization could be performed using any of a variety of nonlinear optimization techniques, for which there is an abundance of literature [e.g., Press et al. (1996)].

However, this method was not used for one main reason. If the gradient of the least-squares cost function with respect to the independent variables (depths) is unknown, as is the case here, it must be determined numerically, in one way or another. Even the best optimization techniques would likely require the Boussinesq model to be run a large number of times to acquire this information. Because performing the Boussinesq computations is by far the greatest burden of the inversion, it would be best to minimize this. A further criticism of this type of method is that it throws away all knowledge that we already have about the behavior of waves that could otherwise have been used to assist in updating the depth. Because of this, a different technique was used, which implicitly assumes a gradient and minimum based on a knowledge of wave mechanics. Convergence to a solution is fast and accurate for a range of cases.

This method is based on one near-universal observation: Waves travel faster in deep water than in shallow water. Therefore, if, at some representative point in the area of interest, the phase speed of the computed wave is less than the phase speed of the measured wave, the local depth should be increased and vice versa.

Long-wave theory even provides an explicit estimate of what the updated depth should be. For a test bathymetry with local depth  $h_1$ , the local phase speed of a wave will be

$$c_1 = \sqrt{gh_1} \quad (3)$$

and at the optimum depth  $h_m$  the measured phase speed from the data will be

$$c_m = \sqrt{gh_m} \quad (4)$$

Because all other quantities are known or can be determined from the data, the optimum depth  $h_m$  can be computed

$$h_m = h_1 \left( \frac{c_m}{c_1} \right)^2 \quad (5)$$

If this calculation is performed at all representative depth points, an updated bathymetry will result for the next Boussinesq run. A particular advantage is that the water depth at the representative points is always positive, which would not be guaranteed by many methods.

Eq. (5) is explicitly valid only for long waves but will converge for a wide range of wavenumbers. However, in intermediate depths, convergence was found to be quite slow; the magnitude of depth change was underestimated significantly at each iteration. Using the full linear dispersion relation, it is possible to construct an alternative to (5) that is valid over the full range of wavenumbers. However, this would require an accurate estimate of either local wavelength or period. If there are any errors in this estimate, there may be no solution for updated depth, in contrast to (5), which always gives a result. Therefore, as a compromise, the exponent in (5) was empirically increased. Essentially, this changes the assumed wavelength from shallow water to somewhere in intermediate depths, while keeping a broad range of convergent wavenumbers. Good results were found using

$$h_m = h_1 \left( \frac{c_m}{c_1} \right)^4 \quad (6)$$

which simply changes the long-wave exponent of 2 to an empirically determined 4. Exponents  $>4$  should not be used, as the method then becomes formally unstable in the long wavelength limit.

One final point is left, which seems somewhat trivial but has enough hidden complexity to deserve a detailed explanation—the computation of phase speed.

## Computation of Phase Speed

The first point of interest in computing phase speeds is readily apparent from (6): It is not necessary to find absolute phase speeds, only the ratio of phase speeds from the measured and computed data. Furthermore, because (6) is approximate and will converge for a range of exponents, it can be inferred that even small errors in this ratio may be tolerated as long as ratios  $<1$  remain  $<1$  and so on.

Local phase speeds thus were measured using 2D cross-correlation coefficients, which provide a stable estimate and are relatively simple to compute. The overall area of interest is first divided into overlapping subdomains. In each subdomain, the cross correlation between the zero-mean initial and final snapshots is found for both the measured and computed data.

If the subdomain snapshots at times  $t = 0$  and  $t = t_1$  are designated as matrices **A** and **B** with grid sizes  $(\Delta x, \Delta y)$ , the cross correlation at lag  $(j\Delta x, k\Delta y)$  is defined here

$$\text{corr}(A, B)_{j,k} = \sum_{m=1}^{M-j} \sum_{n=1}^{N-k} \mathbf{A}_{m+j,n+k} \mathbf{B}_{m,n} \quad (7)$$

where matrix indices are  $(1:M, 1:N)$ .

The cross-correlation matrix will be largest for some matrix lag  $(r, s)$  corresponding to a physical distance  $D = \sqrt{(r\Delta x)^2 + (s\Delta y)^2}$ , which is the distance the wave has traveled in time  $\Delta t$ . The ratio of the measured and computed distances  $D_m/D_1$  is thus the ratio of phase speeds  $c_m/c_1$ . It is generally necessary to use paraboloid interpolation to find the matrix peak to subgrid resolution.

For regular waves, with **M** and **N** very large, cross-correlation peaks will approach the exact phase speed and direction of the wave. For irregular waves, the cross-correlation peak will give some sort of average phase speed, which will be close to that of the peak of the wavenumber spectrum. For irregular waves with large amounts of data, cross correlations may be used to find phase speeds and amplitudes for the full spectrum of wave numbers and directions. However, with the limited data available here and the inversion algorithm used, this property was not used.

A feature of cross correlations that makes them practical is that they may be computed using fast Fourier transforms. (See, e.g., Press et al. (1996), p. 538, for an explanation for 1D processes. The extension to two dimensions is obvious.)

There are several subtleties. If the time lag between snapshots is a small fraction of the dominant wave period, it is simple to automatically determine the distance the wave has traveled. However, at a time lag of around half the dominant wave period, the distance and direction of travel becomes ambiguous—was the wave going forward or backward? This ambiguity will cause unstable errors in the depth inversion algorithm. To resolve this, a dominant direction of travel is established. Wave rays thus are assumed to travel  $<90^\circ$  from some given direction. For most applications this is not a very limiting assumption. Using this, the ambiguity disappears to near the point where a full wavelength has passed through the domain (around one dominant wave period) when a different ambiguity appears. However, in all cases, we will use small enough time lags that this will not be a problem. A time lag of around one-third of the dominant wave period was found to work well.

To get reasonable estimates of phase speed, it is necessary to have enough data, especially when computations are just beginning. For most cases here, subdomains of around 3 wave-

lengths in the dominant direction of travel were used to begin with, and as the iterations began to converge, smaller windows of 1.5–2 wavelengths were used. In some cases, even smaller windows could be used near the final convergence. Window sizes perpendicular to the direction of travel were generally less than a dominant wavelength.

### Correction for Data Mismatches

There is one common situation that, if left uncorrected, can seriously harm the performance of the depth inversion algorithm. This results from possible data mismatches between measured surface elevations and velocities. The problem is shown most easily by example.

Imagine, for simplicity, a 1D wave traveling over a flat bed. The surface elevations and surface velocities will be

$$\eta(x, t) = \eta_0 \cos(x - ct) \quad (8)$$

$$u(x, t) = \eta_0 T_r \cos(x - ct) \quad (9)$$

where  $T_r$  is some transfer function between surface elevation and horizontal surface velocity. Snapshots of this at times  $t = 0$  and  $t = t_1$  are used to initialize the Boussinesq model for an inversion and for computing phase speeds. Now imagine that the remote sensing platform has some error in measuring velocities (results are essentially the same for an assumed error in surface elevation) so that the measured velocity is 10% less

$$u_m(x, t) = 0.9\eta_0 T_r \cos(x - ct) \quad (10)$$

The surface elevations and velocities used to initialize the Boussinesq model at  $t = 0$  thus will be

$$\eta(x, t) = \eta_0 \cos(x) \quad (11)$$

$$u_m(x, t) = 0.9\eta_0 T_r \cos(x) \quad (12)$$

If the Boussinesq model has the correct bathymetry, i.e., the phase speed is correct, the resulting Boussinesq waveform will be

$$\eta(x, t) = 0.95\eta_0 \cos(x - ct) + 0.05\eta_0 \cos(x + ct) \quad (13)$$

$$u_m(x, t) = 0.95\eta_0 T_r \cos(x - ct) - 0.05\eta_0 T_r \cos(x + ct) \quad (14)$$

Because of the data mismatch between  $\eta$  and  $u$ , a spurious free wave now exists in the Boussinesq model that travels in the opposite direction to the actual wave. This could significantly affect the computation of phase speed as determined through cross correlations. Because this spurious wave will not be in the measured data, even when the assumed bathymetry is correct, the ratio of computed to measured phase speeds will not be unity. This leads to unacceptable errors in the inverse bathymetry, as will be shown. Because such mismatches in measured quantities are to be expected, some method must be implemented to account for this if the inversion algorithm is to be useful. Fortunately, there exists a straightforward correction that is both simple and effective.

This correction does not affect the Boussinesq computations; it is simply a way for canceling out most of the spurious free wave when computing phase speed after the Boussinesq model is finished. It makes use of the observation that waves traveling in the positive  $x$ -direction have surface elevations and velocities with identical phase, and those traveling in the negative  $x$ -direction have opposite phase. Before introducing the correction, we will first replace the assumed value 0.9 in (10) with the more generalized value  $F$  and also introduce a phase error  $\delta$ . The resulting Boussinesq waveform becomes

$$\eta(x, t) = \eta_0 \left[ \frac{1 + F \cos \delta}{2} \cos(x - ct) + \frac{1 - F \cos \delta}{2} \cos(x + ct) + \frac{F \sin \delta}{2} \sin(x - ct) - \frac{F \sin \delta}{2} \sin(x + ct) \right] \quad (15)$$

$$u(x, t) = \eta_0 T_r \left[ \frac{1 + F \cos \delta}{2} \cos(x - ct) - \frac{1 - F \cos \delta}{2} \cos(x + ct) + \frac{F \sin \delta}{2} \sin(x - ct) + \frac{F \sin \delta}{2} \sin(x + ct) \right] \quad (16)$$

where the values of  $F$  and  $\delta$  are unknown.

At time  $t = 0$  the amplitudes of the surface elevations and velocities may be estimated from the data as  $\eta_0$  and  $F\eta_0 T_r$ , using standard deviations or any other desired technique. Next, the means are removed from both surface elevation and velocity (not required in this example, but necessary in more complicated cases with setups and mean flows). The free surface velocity [(16)] is then multiplied by  $\eta_0/F\eta_0 T_r$ , and added to the free surface elevation [(15)] to get

$$Q = \eta_0 \left[ \frac{1 + F \cos \delta}{2} \left( 1 + \frac{1}{F} \right) \cos(x - ct) + \frac{1 - F \cos \delta}{2} \left( 1 - \frac{1}{F} \right) \cos(x + ct) + \frac{F \sin \delta}{2} \left( 1 + \frac{1}{F} \right) \sin(x - ct) - \frac{F \sin \delta}{2} \left( 1 - \frac{1}{F} \right) \sin(x + ct) \right] \quad (17)$$

With this transformed quantity, the magnitude of the forward wave is increased, and that of the backward wave is decreased. The ratio of these two quantities is easily seen to be

$$\frac{|\eta_{fwd}|}{|\eta_{back}|} = \frac{\left( \left( 1 + \frac{1}{F} \right) \sqrt{(1 + F \cos \delta)^2 + (F \sin \delta)^2} \right)}{\left( \left( 1 - \frac{1}{F} \right) \sqrt{(1 - F \cos \delta)^2 + (F \sin \delta)^2} \right)} \quad (18)$$

which is improved from the original [(15)]

$$\frac{|\eta_{fwd}|}{|\eta_{back}|} = \frac{\sqrt{(1 + F \cos \delta)^2 + (F \sin \delta)^2}}{\sqrt{(1 - F \cos \delta)^2 + (F \sin \delta)^2}} \quad (19)$$

Fig. 3 shows the magnitude of the ratio of forward to backward wave before and after the transform. The improvement is striking. It must be emphasized that no prior knowledge was

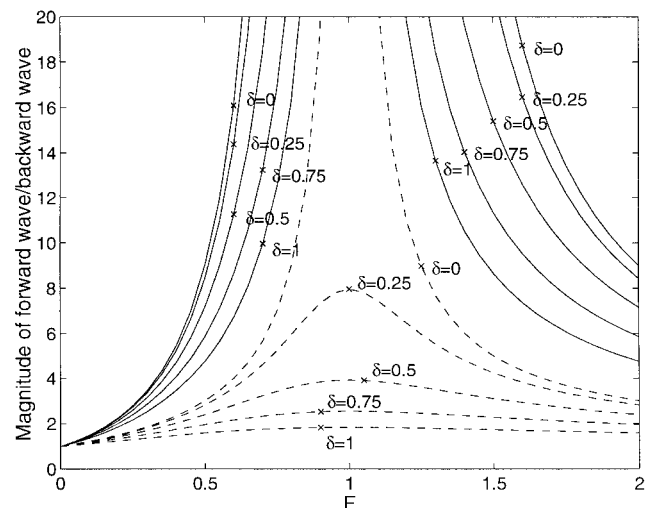


FIG. 3. Relative Magnitudes of Forward and Backward Waves for Varying Amplitude  $F$  and Phase  $\delta$  Errors [(-) No Data Correction; (---) after Data Correction Applied]

needed to improve the data, only that the mismatch not be large. In computations, the quantity

$$Q = \eta + (\eta_0/u_0)u \quad (20)$$

which is equivalent to (17), was used as the input quantity for cross correlations. In any window, both  $\eta_0$  and  $u_0$  were taken to be the standard deviations of the data in that window, and  $\eta$  and  $u$  had the mean removed.

For 2D waves, surface velocity in the direction of wave propagation should be used as the representative velocity in (20), as this maintains the necessary identical phase-opposite phase character. It is straightforward to show that the performance of the transform is insensitive to small errors in the assumed direction of travel, which is an important result for multidirectional seas. Broadbandness of the wave spectrum, nonlinearity, and real reflected waves in the data will act to decrease somewhat the effectiveness of the transformation, but significant improvements still will be gained. Based on present experience, it should always be used.

## INVERSION TESTS

### Implementation of Inversion Algorithm

To implement the inversion algorithm, representative points were chosen on a rectangular grid over the area considered. Depths were defined as these points and were interpolated elsewhere using 2D, cubic B-splines. Depth updates were performed only at these representative points. It was found that, to decrease short wavelength oscillations, depth updates should be spread somewhat across adjacent representative points. If the new depths are written

$$h_{new} = h_{old} + (h_{new} - h_{old}) \quad (21)$$

then the quantity  $h_{new} - h_{old}$  was filtered at each representative point using a 2D nine-point filter before being applied.

Due to the present unavailability of suitable field data, the inversion algorithm was tested for a number of different bathymetries using "synthetic field data" generated by a Boussinesq model. Tests started using regular waves over simple bathymetries and progressed to more difficult cases of irregular waves over complex bathymetries with strong currents.

For all cases, a minimum depth was specified to prevent possible problems if the depth were to become too small. Input data for computations also used a minimum depth, so no real shoreline existed in any tests. For use very near the shoreline, special techniques would need to be developed. The inversion also specified that, beyond a certain point offshore, the bathymetry was constant. This was done to avoid extrapolating depths and represents another small limitation. Finally, for 2D bathymetries, the inversion algorithm was allowed to know that sidewalls existed, which would not be the case for field data.

These special conditions were imposed simply to allow a greater use of the available data near the boundaries. For use with field data, they would need to be modified for most cases. However, they do nothing to help or inhibit the depth inversion algorithm, which is the main focus of this paper.

### Regular Waves over Plane Slope

For a first test, the inversion technique was run for the case of regular waves over a 1D plane slope. Input data was generated by a Boussinesq model, which was run until it reached a steady state solution. Input waves were approximately 10 cm in height at depth  $h = 0.3725$  m with period 1 s [ $(kh)_0 \approx 1.5$ ,  $(H/h_0) = 0.27$ ]. Surface elevations and horizontal velocities were output at two intervals separated by 0.375 s ( $\Delta t/T = 0.375$ ) with 0.05 m spatial resolution. Fifteen evenly spaced

representative points were used by the inversion algorithm to represent the depth variation. The ends of the domain were not used due to the effects of sponge layers and wave generators in the input data, which were used to generate and absorb waves in the Boussinesq model. These are computational artifacts that do not appear in field data, and thus field inversions could proceed much closer to the data boundaries. Window sizes used for cross correlations varied from 3.15 m at the first iteration to 1.55 m by the last iteration.

Fig. 4 shows true and inverse bathymetries after 12 iterations of the depth updating algorithm. Agreement between the two bathymetries is very good, with an RMS error of 0.040, normalized by the local depth. Because the same model that was used to generate the data also ran the wave driver in the inversion, agreement should be very good if the inverse algorithm is to be useful. Thus, all of these tests should be seen as more a test of the inversion algorithm, which can be used with any appropriate wave driver, than of the absolute accuracy of the Boussinesq model-inversion system.

Differences between predicted and input bathymetries are seen in the breaking zone and at the two abrupt changes in slope, which slowed convergence. These abrupt breaks, which are relatively uncommon on sandy topographies, could not be modeled well by the cubic spline that was used to interpolate between representative depth points. However, the differences in the breaking zone, which had a maximum relative error of 0.10, are structural and appeared in all tests where waves broke. Using only surface elevations and velocities as input, it is not possible to completely specify history-dependent wave-breaking parameters when the Boussinesq model is initialized. Because of this, inversion runs always assumed that waves were nonbreaking at the beginning of computations. Because in reality, the waves may have been breaking, differences appear.

Initial convergence was very fast. After five iterations, values differed from the final answer by <10%. A qualitatively similar pattern was found in all cases tested, where initial convergence was quick, followed by a slowdown as the model tried to fit the detailed features.

The previous test used perfect data as input. However, as mentioned previously, exact data cannot be guaranteed. Fig. 5 shows results from two inversions using input velocities that were 0.9 of the exact value ( $F = 0.9$ ,  $\delta = 0$ ), with all other quantities the same. When the correction for data mismatches [(20)] was used, agreement is very good, with an RMS error of 0.049, which is only slightly worse than when perfect data is used. However, when (20) is not used, agreement becomes

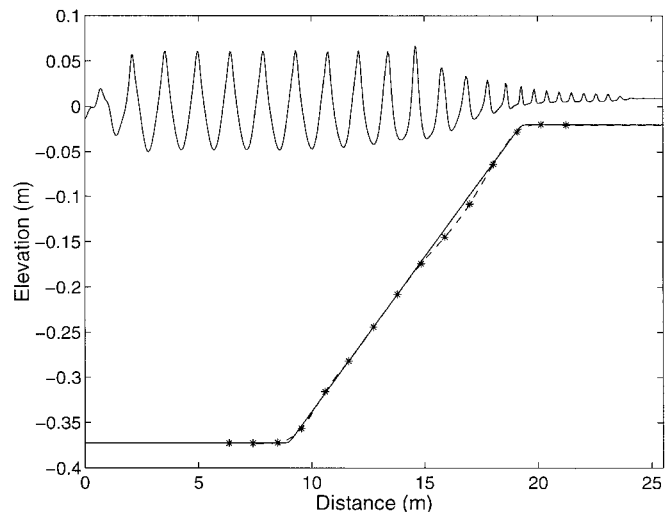


FIG. 4. Input (—) and Inverse (--) Bathymetries over Plane Slope, Showing Locations of Representative Depth Points (\*)

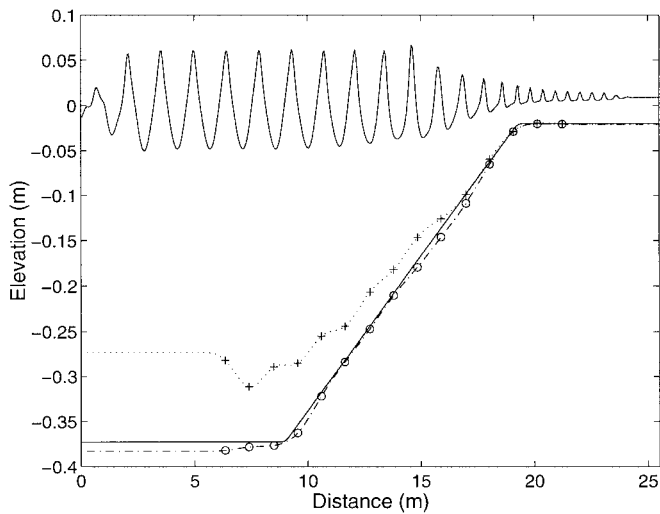


FIG. 5. Input (—) and Inverse Bathymetries over Plane Slope, with 10% Error in Input Velocities, ( $\cdots + \cdots$ ) No Data Correction; ( $-\circ-\circ-$ ) Using Correction

very poor, with an RMS error of 0.140. The spurious free waves introduced by the mismatch in elevations and velocities have affected the estimates of phase speed to such an extent that depth estimates are unusable. This is why (20) should always be used to condition the data before phase speeds are calculated.

### Regular Waves over Elliptical Shoal

For a more demanding test, the inverse bathymetry was calculated for the case of an elliptical shoal on a plane slope. This used the well-known experimental bathymetry and conditions of Berkhoff et al. (1982) as input. Regular waves with period of 1 s and initial height  $H = 0.0464$  m were generated in a depth of 0.45 m [ $(kh)_0 \approx 1.9$ ,  $(H/h)_0 = 0.103$ ] and shoaled onto a plane slope that was at an angle of  $20^\circ$  to the waves.

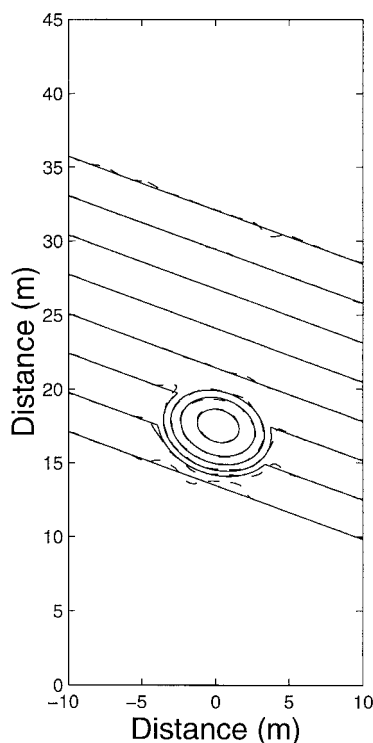


FIG. 6. Input (—) and Inverse ( $-\circ-$ ) Contours over Berkhoff et al. (1982) Shoal

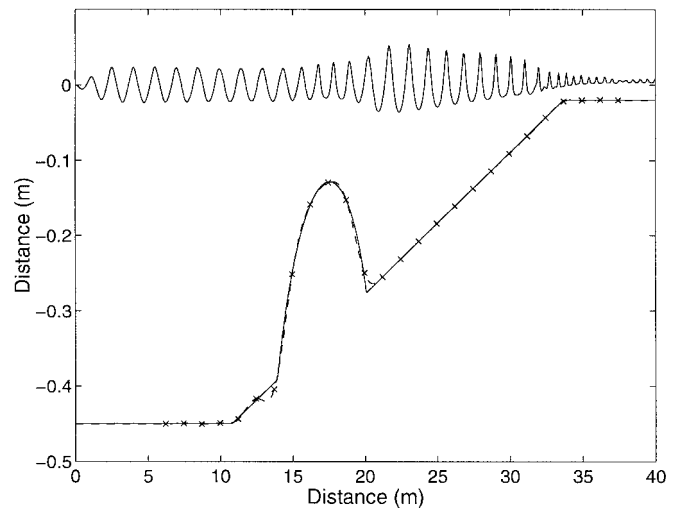


FIG. 7. Input (—) and Inverse ( $-\circ-$ ) Cross Section through Berkhoff et al. (1982) Shoal at  $y = 0$

On the slope was an elliptical shoal that acted as a strong focus. This case was also considered by Dalrymple et al. (1998), who found good agreement using linear inversion techniques, with input data from a parabolic model.

For the inversion, once again two snapshots of surface elevations and velocities separated by 0.375 s ( $\Delta t/T = 0.375$ ) were used. In the cross-shore direction, 26 representative points were used, and in the longshore direction, 20 points were evenly spaced over the entire width.

Fig. 6 shows contours of the exact and inverse bathymetries. Once again, agreement between computed and exact values is extremely good, even on the shoal. The relative error in depth, with an RMS value of 0.035, is concentrated at the changes in slope. Some slowness to converge was noted in the deeper section of the simulation, and the topography shown here is after 24 iterations. The deepest depth, with  $kh \approx 1.9$ , is really too large for practical purposes, as the wavelength is only a few percent from its deep water value, and small errors in spatial dimensions would lead to very large errors in depth.

Fig. 7 shows a cross section through the elliptical shoal at  $y = 0$ . The good fit gives greater confidence that the inversion algorithm will work well, even for complex bathymetries. In areas of sharp changes in slope, however, differences are visible.

### Waves over Rip Current Topography

The previous tests, which all showed good performance for the depth inversion algorithm, involved both breaking and nonbreaking waves, but had small currents. However, in real coastal topographies, significant longshore and cross-shore currents may exist. For methods that only look at surface elevations to determine topography [e.g., Grilli (1998)], the effect of these currents on waves will be misinterpreted. However, because the present algorithm uses surface velocity information, it should be able to account correctly for the effects of currents on waves.

Therefore, inversion tests were performed over a bar-trough topography with a rip current channel as shown in Fig. 8. This topography was like the plane slope tested earlier but added a bar with a rip current channel near the shoreline similar to that of Chen et al. (1999). Regular waves with period  $T = 1$  s and height  $H = 0.024$  m [ $(kh)_0 \approx 1.5$ ,  $(H/h)_0 = 0.064$ ] broke on the bar and created a strong current through the rip channel. Two snapshots of surface elevations and velocities spaced at an interval of 0.375 s were used to initialize the Boussinesq model.

A grid of 18 by 15 depth points was used in the longshore and cross-shore directions, respectively. Window sizes in the cross-shore direction varied with the iteration number, from 3.15 m at the first iteration to 1.55 m at the end, and the longshore window size varied from 2.325 to 0.525 m.

Fig. 9 shows a 3D representation of the reconstructed topography. The bar-trough system with the rip channel is seen clearly. The bathymetry had essentially converged after 12 iterations. For the final few iterations, windows with size around 1 wavelength were used to try to get finer resolution. For most of the domain, agreement is very good, but the amplitude of the bar-trough system is significantly underpredicted. The relative RMS depth error for the entire system was 0.052, with almost all of this concentrated near the bar.

Fig. 10 shows a cross section through the bar at  $y = 0$  m, which again shows the underprediction of the bar amplitude. This is believed to be due to two reasons. The first is simply that the bar has features on the order of 1 wavelength, which makes it difficult to resolve accurately. It seems plausible that using more representative depth points in the cross-shore direction would solve this problem, but it was found that too many depth points caused short wavelength instabilities in the bottom topography. The second reason for the differences is that strong wave breaking occurs on the bar. As seen when performing inversions over a plane slope, this leads to an overprediction of depth. However, although fine-scale features

are somewhat smeared, the essentials of the bar-trough rip-channel system are well recognized.

In the bar region, currents were very strong. Fig. 11 shows a portion of the surface velocity snapshot used to initialize the Boussinesq model. The strong rip current and highly irregular velocity field are clearly visible. The effect of these currents is automatically included in the inversion.

Until now, all test scenarios for inversion have used regular waves. However, for a sea state that is not completely confused, it is still possible to determine a dominant phase speed, and the inversion can proceed as normal. Inversions thus were found from an irregular, multidirectional simulation, with peak period and  $H_{RMS}$  identical to the previous test. Because of the unsteady, multidirectional waves, and a strong, chaotically oscillating rip current, at any particular time, water surface elevations and free surface velocities might be very different from those at any previous or future time. Therefore, inversions at one time could differ somewhat from inversions using a different sequence of snapshots. To determine what this variability might be, several inversions were performed at widely spaced time intervals and compared.

Overall, the relative RMS error averaged over the four tests was 0.067. It was found that in the deeper section, results for all irregular tests were almost identical to the input bathymetry. However, near the bar, where the unsteady currents were

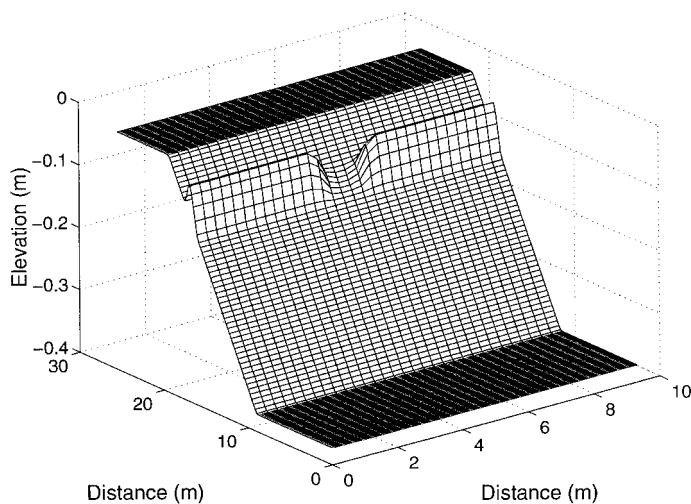


FIG. 8. 3D View of Input Rip Current Topography

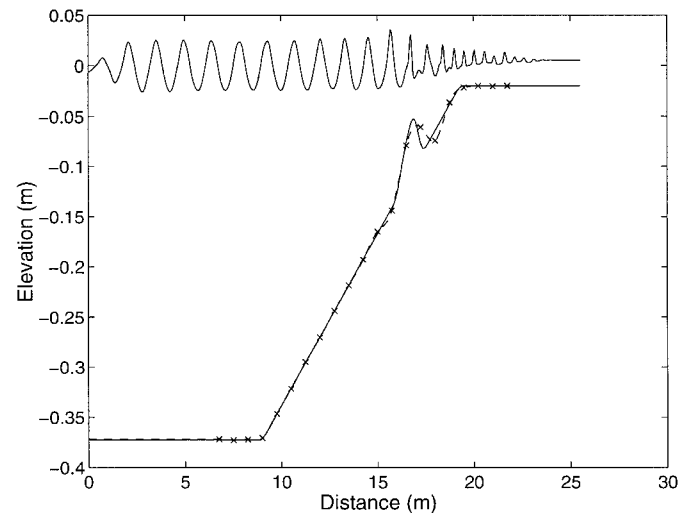


FIG. 10. Input (—) and Inverse (--) Cross Section through Rip Current Topography

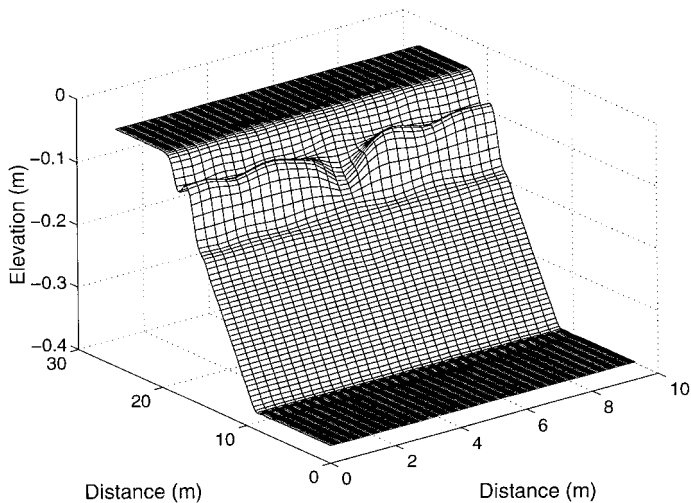


FIG. 9. 3D View of Reconstructed Rip Current Topography, Showing Bar-Trough System and Rip Current Channel

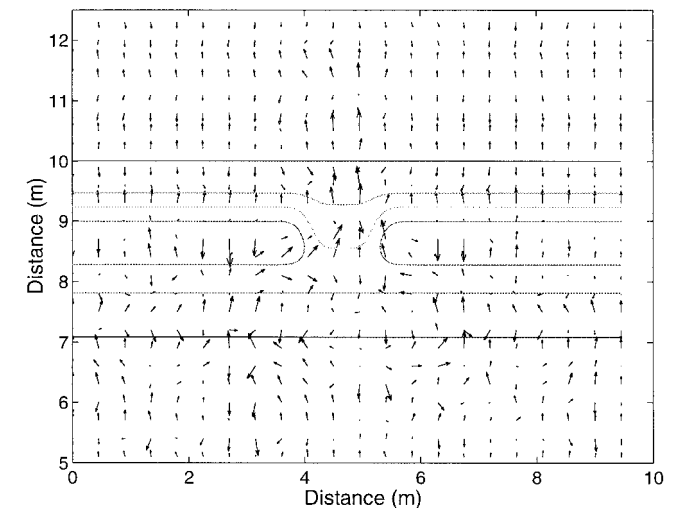


FIG. 11. Instantaneous Velocity Field in Vicinity of Bar, Showing Some Underlying Depth Contours

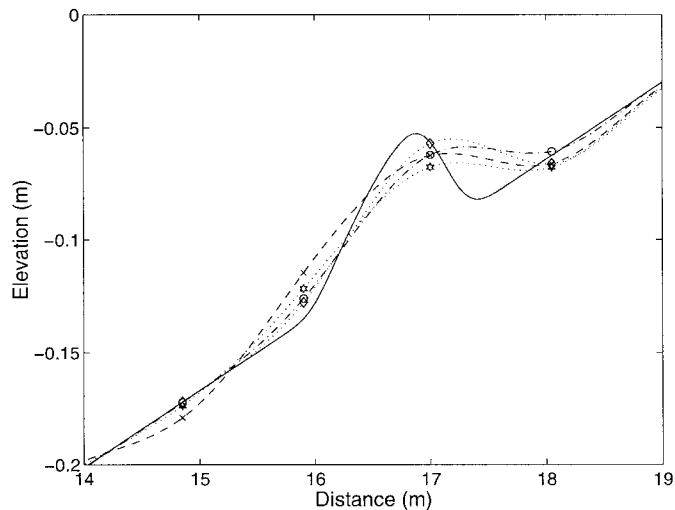
strongest, errors were largest, and some differences did appear between inversions. Even in the same run, long-shore non-uniformities could appear in the inverse bar where none existed in the input bathymetry.

Fig. 12 shows a cross section at  $y = 2.25$  m, showing the results of the four inversions. Results are similar in that they underpredict the amplitude of the bar-trough system, but the details differ. This is believed to be due to the different breaking conditions and currents at each inversion time, which cause the error to take a slightly different form.

However, Fig. 13, which shows the full 3D topography for the first irregular run, still reconstructs clearly the bar-trough, rip-channel system, as did all of the tests.

It was found that irregularity and multidirectionality made it necessary to use larger window sizes and fewer representative points when calculating phase speed. Only 15 points were used in both directions, and window sizes were also larger. Window sizes also depended somewhat on the particular time when the snapshots were taken.

Although this was expected, it still involved some additional trial and error in the inversion. In particular, choosing the number of representative depth points and window sizes for irregular waves was found to be more of an art than a science. Using a small window size while the inversion was still far from convergence was at times found to lead to explosive



**FIG. 12. Cross Section through Bar for Several Inversions Using Irregular Waves [(—) Exact; Dashes, Dots, and Symbols Show Inversions Computed at Widely Spaced Times]**

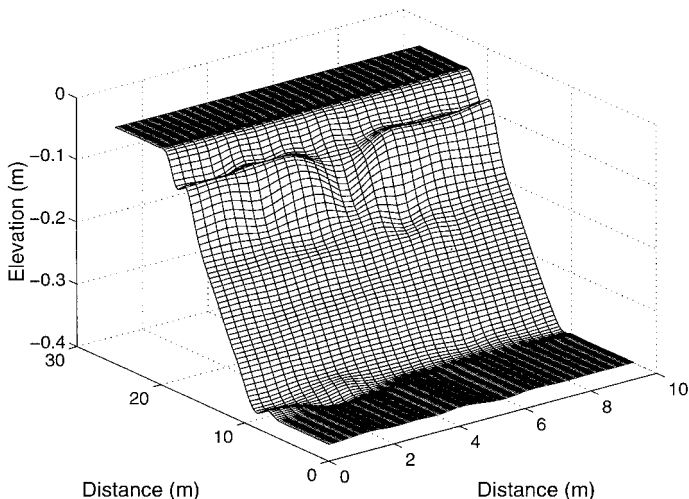


**FIG. 13. 3D View of Reconstructed Rip Current Topography, with Irregular Waves as Input**

instabilities. A visual examination of the areas where this occurred showed that, in these particular windows, shorter waves dominated. If the depth were not close to the exact value, these waves could trick the algorithm used to calculate phase speed. Using larger window sizes until the inversion was nearer convergence solved this problem. However, because larger window sizes lead to slower convergence, this increased the number of iterations necessary. Up to 36 iterations were necessary, depending on the particular features at the instants the snapshots were taken.

## DISCUSSION AND CONCLUSIONS

For inversion using actual field data instead of the synthetic data used here, the principles would remain unchanged, but the details of the implementation would differ somewhat. In particular, the shoreline and boundary conditions would need to be adjusted to fit the physical situation. This would probably mean that the inversion could proceed only until some finite distance from the shoreline or data boundary. It is difficult to tell in advance what loss of accuracy would result near these boundaries.

Another concern would be the quality and availability of data. As of today, no platform known to the authors is capable of remotely sensing accurately surface elevation plus the two horizontal components of surface velocity. Likely, one or more quantities would have to be inferred. Although ways to do this are being examined by the authors, it does introduce another source of error. Fortunately, the data conditioning algorithm [(20)] was found to provide a good solution for the data mismatches that could result.

A further potential source of inaccuracy is horizontal vorticity in the water column, which is not included in the Boussinesq model and, in any case, is impossible to detect using only surface information. For example, surface drift caused by wind stresses will be interpreted by the inversion as a depth uniform current that would have some effect on the waves. However, it would in reality be confined to the top portion of the water column and affect wave motion very little. Again, the effect of this on field inversions remains to be seen.

Although the Boussinesq model of Wei et al. (1995) was used as the basis for the inversions, the inversion methodology is not tied any particular wave driver. If a surf zone model were developed that had, for example, more accurate shoaling near the breaking point or better nonlinear dispersion than the present model, this could be used instead. The accuracy of field inversions would certainly improve with increasing wave model accuracy, but the degree of improvement remains to be seen. As was mentioned earlier, this paper should be seen as a test of the inversion methodology, rather than the absolute accuracy of the combined methodology/wave-driver system.

In conclusion, for a variety of topographies, with regular or irregular waves, and in the presence of strong currents, the inversion methodology presented here has been found to converge to near the ideal solution. However, several areas exist where inaccuracies can be found. Firstly, in areas with abrupt changes in topography, the inversion will not be able to reconstruct the sharp detail. Secondly, because it is not possible to pass full information about breaking to the model, some error may be found in the breaking zone. Finally, if the data improvement technique given here is not used, even small errors in data may lead to large errors in inferred depth. However, if this technique is used, these errors become minimal.

## ACKNOWLEDGEMENTS

This work was supported by the Office of Naval Research, Base Enhancement Program, through Grant N00014-97-1-0283.

## APPENDIX. REFERENCES

- Berkhoff, J. C. W., Booy, N., and Radder, A. C. (1982). "Verification of numerical wave propagation models for simple harmonic linear water waves." *Coast. Engrg.*, 6, 255–279.
- Chen, Q., Dalrymple, R. A., Kirby, J. T., Kennedy, A. B., and Haller, M. C. (1999). "Boussinesq modelling of a rip current system." *J. Geophys. Res.*, 104(9), 20,617–20,637.
- Chen, Q., Kirby, J. T., Dalrymple, R. A., Kennedy, A. B., and Chawla, A. (2000). "Boussinesq modeling of wave transformation, breaking, and runup. II: 2D." *J. Wtrwy., Port, Coast., and Oc. Engrg.*, ASCE, 126(1), 48–56.
- Dalrymple, R. A., Kennedy, A. B., Kirby, J.T., and Chen, Q. (1998). "Determining bathymetry from remotely sensed images." *Proc., 26th Int. Conf. Coast. Engrg.*, 2395–2408.
- Dugan, J. P., Suzukawa, H. H., Forsyth, C. P., and Farber, M. S. (1996). "Ocean wave dispersion surface measured with airborne IR imaging system." *Proc., 1995 Int. Geoscience and Remote Sensing Symp. (IGARSS-95)*, 1282–1283.
- Grilli, S. T. (1998). "Depth inversion in shallow water based on nonlinear properties of shoaling periodic waves." *Coast. Engrg.*, 35, 185–209.
- Kennedy, A. B., Chen, Q., Kirby, J. T., and Dalrymple, R. A. (2000). "Boussinesq modeling of wave transformation, breaking, and runup. I: 1D." *J. Wtrwy., Port, Coast., and Oc. Engrg.*, ASCE, 126(1), 39–47.
- Kirby, J. T. (1997). "Nonlinear, dispersive long waves in water of variable depth." *Gravity waves in water of finite depth*, J. N. Hunt, ed., Computational Mechanics Publications, 55–126.
- Madsen, P. A., Sørensen, O. R., and Schäffer, H. A. (1997a). "Surf zone dynamics simulated by a Boussinesq-type model. Part I. Model description and cross-shore motion of regular waves." *Coast. Engrg.*, 32, 255–287.
- Madsen, P. A., Sørensen, O. R., and Schäffer, H. A. (1997b). "Surf zone dynamics simulated by a Boussinesq-type model. Part II. Surf beat and swash oscillations for wave groups and irregular waves." *Coast. Engrg.*, 32, 289–319.
- Nwogu, O. (1993). "An alternative form of the Boussinesq equations for nearshore wave propagation." *J. Wtrwy., Port, Coast., and Oc. Engrg.*, ASCE, 119, 618–638.
- Press, W. H., Teukolsky, S. A., Vetterling, W. T., and Flannery, B. P. (1996). *Numerical recipes in Fortran 77: The art of scientific computing*. Cambridge University Press, London.
- Stockdon, H. F. (1997). "Estimation of wave phase speed and nearshore bathymetry using video techniques." MS thesis, Oregon State University, Corvallis, Oreg.
- Wei, G., Kirby, J. T., Grilli, S. T., and Subramanya, R. (1995). "A fully nonlinear Boussinesq model for surface waves. I. Highly nonlinear, unsteady waves." *J. Fluid Mech.*, Cambridge, U.K., 294, 71–92.
- Wu, J., and Juang, J. T. (1996). "Application of satellite images to the detection of coastal topography." *Proc., 25th Int. Conf. Coast. Engrg.*, 3762–3769.